

COGEAR

MODULE 3:

Modelling of slope behaviour and nonlinear phenomena

Del. No.: 3b.3.6

**Authors: Dupray F., Chao L., Seiphoori A.,
and Laloui, L.**

Laboratory of Soil Mechanics, EPFL

July 12, 2012

ENAC - Faculté Environnement naturel, architectural et construit
LMS - Laboratoire de mécanique des sols

EPFL - LMS
Station 18
CH - 1015 Lausanne

Tél.: +41 (0)21 693 23 15
Fax: +41 (0)21 693 41 53
Web: <http://lms.epfl.ch>



Competence Center Environment and Sustainability

COGEAR: COupled seismogenic GEohazards in Alpine Regions

MODULE 3 – Deliverable 3b.3.6

Modelling of slope behaviour and non-linear phenomena

1D non-linear simulations for a case study in Grächen

Authors: Dr F. Dupray, L. Chao, A. Seiphoori, Prof. L. Laloui

Table of contents

Introduction	3
1 Landslides and earthquakes in Valais.....	3
1.1 Main features about Grächen.....	4
1.1.1 Geology information	5
2 Geo-mechanical models	7
2.1 Modified Hujoux model in <i>CyberQuake</i>	8
2.1.1 Strain-stress relationship	8
2.1.2 Yield limit function	9
2.1.3 Plastic flow	10
2.2 Paraxial element	11
3 One dimensional simulation for Grächen.....	13
3.1 Input seisms characterisation.....	13
3.2 Soil mechanical properties	14
3.3 Tests on constitutive models	15
3.4 Tests on soil materials	16
3.5 Tests on inclinations and bedrocks.....	19
Conclusion.....	20
References	21

Introduction

Local soil conditions have the potential to affect the intensity of damages created by a seism at a given site. These conditions encompass two main aspects, the geometry of the site, also known as the site effect, and the dynamic behaviour of the soil layers. The first aspect is studied especially in the case of bottom of valleys, and that is the case in COGEAR project module 3a. It is less well-known for other situations such as a definite zone of soil on a mountain slope: this aspect is treated in deliverable 3b.3.7. The last aspect, dynamic behaviour of soil layers, or lithological site effect, is the focus point of this report. The non-linearity of soil behaviour has been demonstrated being a key factor to affect ground motion during a seism (López-Caballero 2003; Roullé and Bernardie 2010).

Swiss Seismological Service underlined in the report *Seismic hazard assessment of Switzerland* (Giardini *et al.* 2004) that the region of Valais will continue being a very seismically active zone for example, the village of Grächen. In addition, the site of the village lies on a deep-seated rock movement, and is close to known trajectories of rock avalanches. The evaluation of risks for this particular village is therefore representative of a worst case situation at the scale of Switzerland. The village lies on between 30 and 80 m of soil layers, while rock is apparent above and below the village.

However, it is hard to define the effect of individual factors on slope instability because of their mutual interactions. In addition, dynamic effects of earthquake will significantly increase complexity of slope stability problem. As a consequence, it is needed to understand the dynamic behaviour of soil during a seism in conditions close to the reality. The objective of this specific report is to explore some aspects directly related to soil characteristics in the case of Grächen through 1D simulations of ground motion on a column of soil that is representative of the local situation.

This work is divided into three parts. First, a general view of Valais concerning the situation of landslides and earthquakes is addressed, followed by some specificities of Grächen and borehole information. Secondly, theoretical formulation is put forward to focus on various aspects of soil dynamics in the field of constitutive laws. The third part focuses on numerical simulations and analysis.

1 Landslides and earthquakes in Valais

The region of Valais is considered as one of the two most seismically active regions of Switzerland. It experiences an earthquake with a magnitude 6 or above roughly every 100 years according to an historic study (Fritsche *et al.* 2010). It is also characterized by the mountain slopes where a number of villages are built, and natural hazards, among which soil and rock landslides. The village of Grächen presents those characteristics, being built on a soil slope, subjected to possible rock avalanches, and lying on a very large deep-seated rockslide.

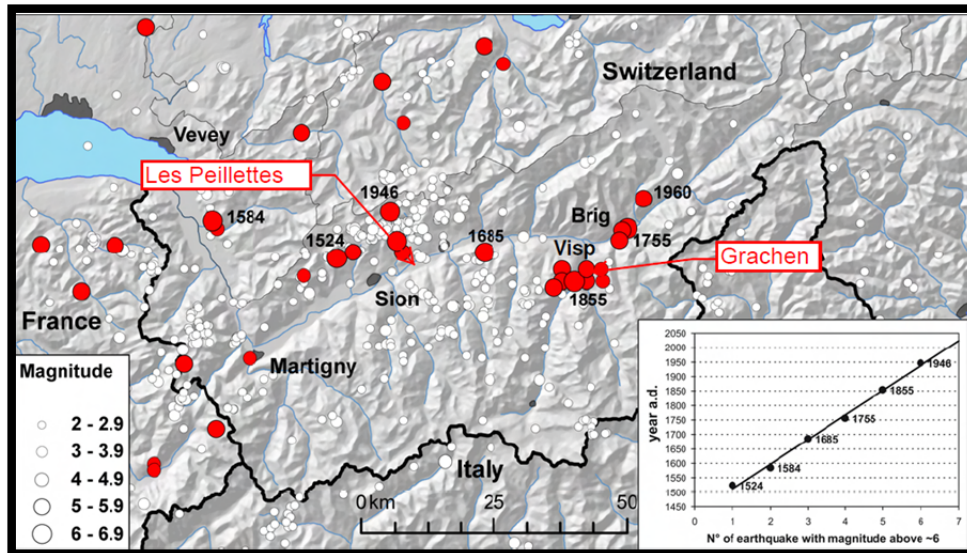


Figure 1: Large earthquakes in the Valais and the timing of magnitude 6 or larger historical events. (Fäh and COGEAR Working Group 2010)

On July 25th, 1855, an earthquake with an intensity of almost VIII (estimated magnitude 6.4) occurred in the region close to Grächen. It triggered a rock avalanche above the village (Jaboyedoff *et al.* 2003). Between Visp and St Niklaus, only one building remained intact. On January 25th, 1946, in the region of Sierre, a magnitude 6.1 earthquake occurred with maximum intensity VIII, which damaged about 4000 buildings, from small fracturing to total collapse. On May 30th in the same year, an intensity of VII earthquake triggered a landslide of 4 to 5 million cubic meters nearby.

These areas experience damages not only from ground motion alone but also secondary effects such as triggered landslides, liquefaction and rock falls. A small scale seismic and frequent shaking will excite failures in steep slopes. Furthermore it will reduce soil strength and influence a lot of stabilities of landslide in long-term, which is also critical to the studied areas.

1.1 Main features about Grächen

Grächen is a mountain village located on the eastern side of Matter Valley (location is indicated in Figure 2), high above the valley at an altitude of about 1600m a.s.l.. Above the village, slopes are forested to 2000m a.s.l. high.



Figure 2: Location of Grächen in the canton of Valais, Switzerland

As shown in Figure 3, the slopes above the village rise up broken rocky terrain to high peaks in permafrost area. The angle of slope, above and below the village, can reach over 30 degree and a mean slope angle of 10 degrees for the village. The whole area seats on a deep-seated rock slide that undergoes translational and roto-translational movement (Noverraz *et al.* 1998).

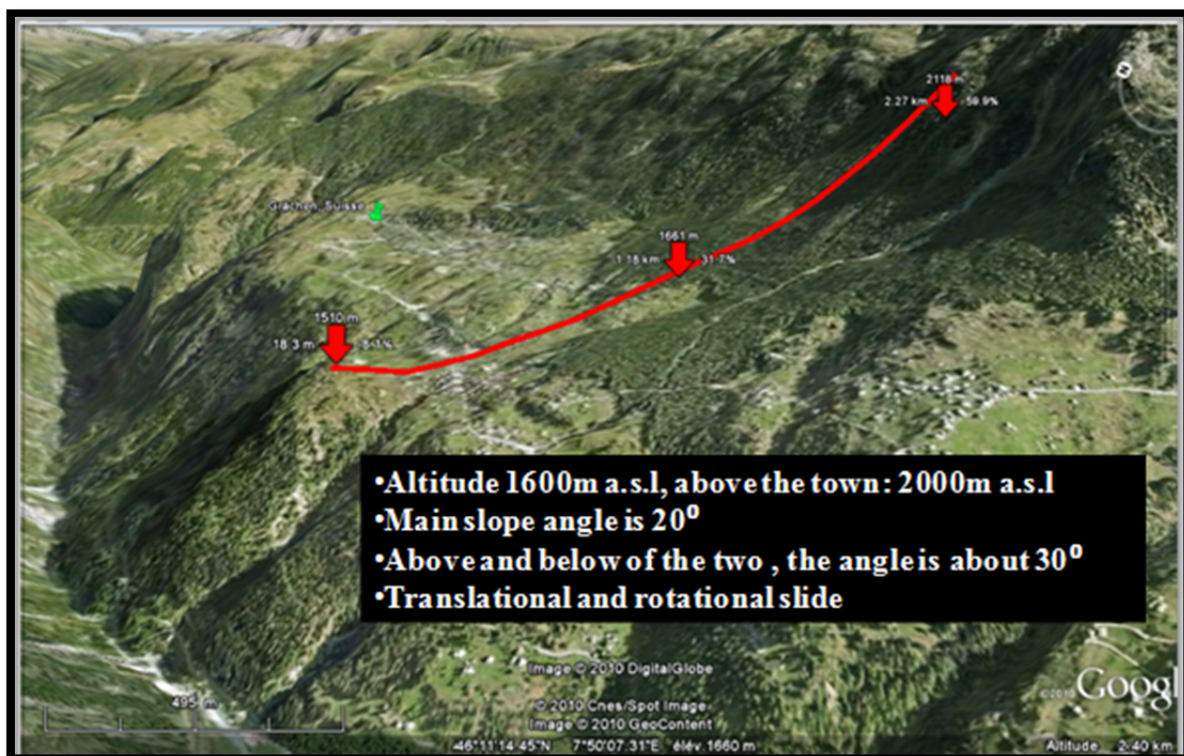


Figure 3: Slope information about Grächen

1.1.1 Geology information

The geology of the site has been investigated in the past for the rock formation (Noverraz *et al.* 1998). But information regarding soil deposits is scarce. Four boreholes were retrieved and are presented by Rovina and Zuber (1997) as well as analysed by Eichenberger *et al.* (2010). Two were selected for this

study due to their location close to the village. Their locations are shown in Figure 4. They only offer a partial view of the area as a whole, but can be used for 1D simulations, with the limitation of an absence of mechanical tests on samples. Mechanical information is gathered through the analysis of ambient noise by high resolution seismic sensors (Burjáněk *et al.* 2010).

Depth (m)	Profile 1(Borehole SB1Meisen)	Depth (m)	Profile 2(Borehole FB2 Meisen)
0-7	Silty sand, gravel, rock fragments, dry	0-7	Silty gravel, rock fragments, dry
7-17	Silty gravel, rock fragments, dry	7-42	Very silty sand, silt, dry – lacustrine deposits
17-22	Very silty sand, gravel, rock fragments, dry	42 – 57	Silty gravel and sand, no rock fragments, wet
22-50	Very silty sand, silt, dry , no rock fragments – lacustrine deposits, dry	57-62	Non-cohesive silty sand, no gravel, wet
		62-76	Silty sand, wet

Table 1: Description of selected boreholes in Grächen

The first selected borehole was bored to 50 m, until rock was found. Four soil formations were identified along the borehole. Below the surface, first 7 meters are made up of a dry layer of silty sand with abundance of gravel and rock fragments. The following 10 meter layer is a moraine formation of silty gravel with lots of sands and rock fragments. Next 5 meters is a dry layer of ground moraine with very silty sands, gravels and many rock fragments. The last 28 m consist of fine-grained lacustrine deposits and contain varied types of deposits, from very silty and fine sand to silt deposits. The specificity of this borehole is the presence of this thick layer of low quality soil without large fragments. That kind of soil is expected to exhibit a very plastic behaviour. All layers found in this borehole have a low permeability, due to high silty content.

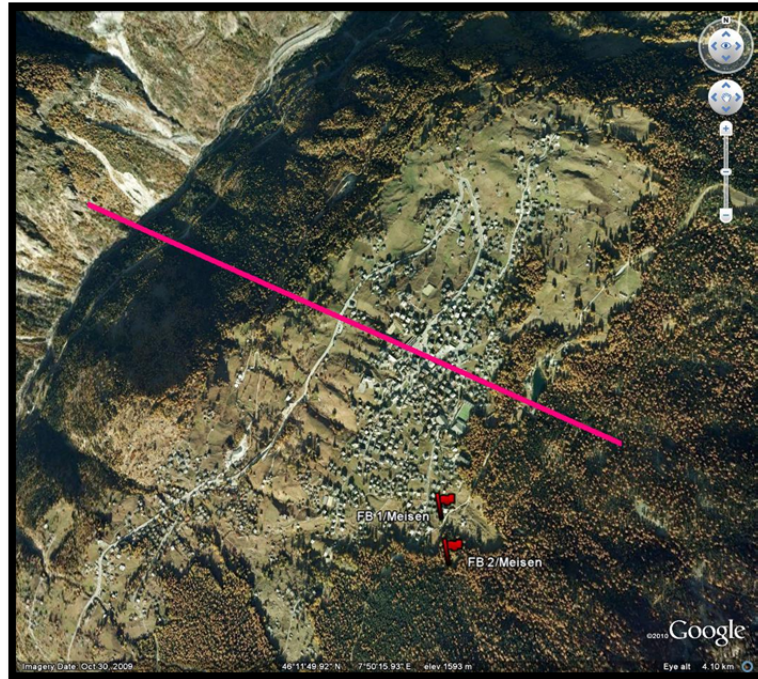


Figure 4: Location of the boreholes (red flags) and geology cross section (see Del. 3b.3.7)

The other selected borehole in Meisen is 16 meters longer than the first one. First layer of 7 meters contains a formation of moraine that is similar in composition and thickness to the second layer of the first borehole. Next, a 35 meters deep layer of fine-grained lacustrine deposits contains not only silty sand with gravel but also angular schist. This is comparable to the fourth layer of the first borehole, though with more fragments. From 42 to 57 meters, silty gravel and sand have been found with no rock fragments. In addition, this layer starts to be wet. The following 5 meters contain non cohesive silty sand without gravel. Also this layer is wet. The last 14 meter layer is made up of weak and wet silty-sand.

From these 2 boreholes, it is observed that in and above the fine grained lacustrine layer, the soil is always dry and lowly permeable. Moreover in the second borehole, just below this layer, the aquifer probably located at depth of about 42 meters. In addition, the layers located at and under aquifer contains amount of loose materials, which is dominant in terms of risk of cyclic liquefaction in seismic scenario.

2 Geo-mechanical models

In order to simulate the soil behaviour, appropriate software should have the capacity to take into account the non-linear behaviour of soil deposits in analysis of strong motion earthquakes. In the case of dynamic analysis, not only constitutive laws for seismic loading should be taken into account, but also the capacity to simulate the boundary conditions should be paid attention. Seismic waves will be reflected by artificial domain boundaries if they are not designed for dynamic analysis, which will lead to an over-estimation of site response.

Because of available borehole information of Grächen, one-dimensional analysis is decided to carry out in order to reproduce the main characteristics of material response. *CyberQuake* is selected for this type of analysis. The program was developed at BRGM by Modaressi and Foerster (2000). A simplified numerical approach basing on Hujoux-type model proposed by Modaressi and Mellal has

been implemented recently in the *CyberQuake* (Mellal 1997). *CyberQuake* is optimized for one dimensional geometry problems and it provides a good tool such as deformable bedrock to obtain response of a multi-layer soil column under earthquake loading. Roullé and Bernardie (2010) compared simulated results to observation data. They concluded that *CyberQuake* is capable of reproducing the main characteristics of soil response in terms of duration, energy distribution, amplitude and frequency content. This program proposes to use a constitutive soil model, the modified Hujieux model, that is designed specifically for dynamic analysis. In this section, important features of this model such as both monotonic and cyclic soil behaviours, hydro-mechanical coupling and boundary conditions are addressed.

2.1 Modified Hujieux model in *CyberQuake*

Mellal (1997) optimized the Hujieux multi-mechanisms model (Aubry *et al.* 1982; Hujieux 1985) for one dimensional analysis. The formulation of this 1D optimization is addressed in the following paragraphs.

2.1.1 Strain-stress relationship

The soil is considered as an isotropic material in the Hujieux model. In the very small range of deformation, the behaviour of soil is elastic and reversible. The following equations are written for the considered case, i.e. a 1D geometry, on a potential sliding plane. The relationship of the incremental elastic deformation with the normal effective stress σ'_n and the shear effective stress vector $\underline{\tau}$ is given by:

$$\begin{cases} d\sigma'_n = (\lambda + 2\mu)d\varepsilon_n^e \\ d\underline{\tau} = \mu d\underline{\gamma}^e \end{cases} \quad [1]$$

in which ε_n^e and $\underline{\gamma}^e$ are the normal elastic strain and the shear elastic strain vector, λ and μ are the Lamé parameters. In the elastic medium, the propagating velocities of S wave and P wave are related to this 2 parameters: $\mu = \rho v_s^2$ and $\lambda + 2\mu = \rho v_p^2$, ρ being the density of the material. The total strain is decomposed into reversible and irreversible parts:

$$\begin{cases} d\varepsilon_n = d\varepsilon_n^e + d\varepsilon_n^p \\ d\underline{\gamma} = d\underline{\gamma}^e + d\underline{\gamma}^p \end{cases} \quad [2]$$

Where ε_n^p and $\underline{\gamma}^p$ are the normal plastic strain and the shear plastic strain vector. Combining with [1] :

$$\begin{cases} d\sigma'_n = (\lambda + 2\mu)(d\varepsilon_n - d\varepsilon_n^p) \\ d\underline{\tau} = \mu(d\underline{\gamma} - d\underline{\gamma}^p) \end{cases} \quad [3]$$

2.1.2 Yield limit function

The yield function is based on Mohr-Coulomb criterion $\|\underline{\tau}\| = -\sigma'_n \tan \phi$ whose general form is $\|\underline{\tau}\| + \sigma'_n F |r| = 0$, where the variable r and the function F allow to take into account the isotropic volumetric hardening or softening.

For both cyclic loading and monotonous loading, the yield limit surface function is defined as,

$$f = \left\| \underline{\tau} - \frac{\sigma'_n F}{\sigma'_{n0} F_0} \underline{\tau}_0 \right\| + \sigma'_n F |r - r_0| \quad [4]$$

The index \bullet_0 is the value of the last loading or unloading. This formulation is then also valid for the first loading, in which $\underline{\tau}_0$ and r_0 are zero.

The function F controls the isotropic hardening and softening by means of the plastic strain and critical state of the material:

$$F = 1 - b \left(\ln \frac{\sigma'_n}{\sigma'_{c0}} - \beta \varepsilon_n^p \right) \quad [5]$$

Where β is the plastic compressibility modulus and σ'_{c0} is the critical state pressure for the initial state and b is a numerical parameter. The parameter b depends on the material of soil and it presents the form of the yield surface in the deviatoric normal stress plan. Its value varies from 0 to 1, the yield surface will pass from a Mohr-Coulomb type surface to a Cam-clay yield surface as shown in Figure 5: .

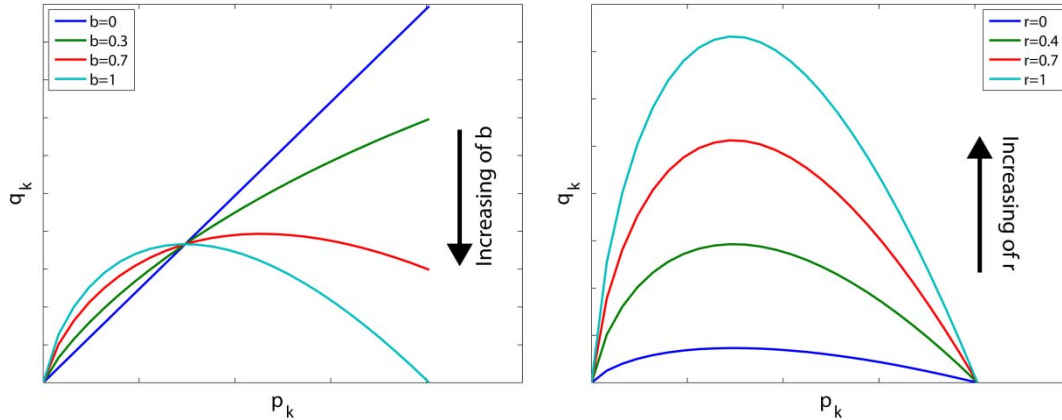


Figure 5: Influence of the numerical parameter (b) and the degree of mobilized friction (r) on the yield surface shape.

The internal variable r introduces the effect of shear strain on the hardening of the soil. It depends on the plastic shear strain $\underline{\gamma}^p$. The expression of r is:

$$r = r_0 - (r_m + r_0) \left(\frac{(\gamma^p - \gamma_0^p)}{\frac{|r - r_0|}{E_p} + (\gamma^p - \gamma_0^p)} \right)^{n_r} \quad \text{with } r_m = \begin{cases} \tan \phi & \text{loading or reloading} \\ -\tan \phi & \text{unloading} \end{cases} \quad [6]$$

where γ^p is the sum of the norms of plastic shear strains during the loading, $\gamma^p = \int_0^t \|d\gamma^p\| dt$, t being the current time. γ_0^p is the sum of the norms of plastic shear strains at the time of the last change in direction of load or reload t_0 , $\gamma_0^p = \int_0^{t_0} \|d\gamma^p\| dt$. The parameters n_r and E_p are the model parameters governing the evolution of the yield surface towards the total plastic mobilization. ϕ is the friction angle at the critical state.

2.1.3 Plastic flow

Plastic volumetric strains and plastic shear strains are evaluated by Roscoe's dilatancy rule:

$$\begin{cases} d\boldsymbol{\varepsilon}^p = d\lambda^p \boldsymbol{\Psi}_v \\ d\boldsymbol{\gamma}^p = d\lambda^p \boldsymbol{\Psi}_d \end{cases} \quad [7]$$

where $d\lambda$ is the plastic multiplier which is determined by the consistency condition.

The direction of plastic flow are obtained by the normality rule for the deviatoric component and Roscoe's dilatancy rule for the normal plastic strain,

$$\begin{aligned} \Psi_v &= -\alpha_\psi \zeta(r) (\tan \psi - F |r - r_0|) \\ \Psi_d &= \partial_\tau f \end{aligned} \quad [8]$$

in which ψ is the slope of the characteristic line as shown in Figure 6. This line defines the change from a contracting to a dilatant behaviour, dilatancy being over the characteristic line. α_ψ is a parameter influencing the amplitude of dilatancy.

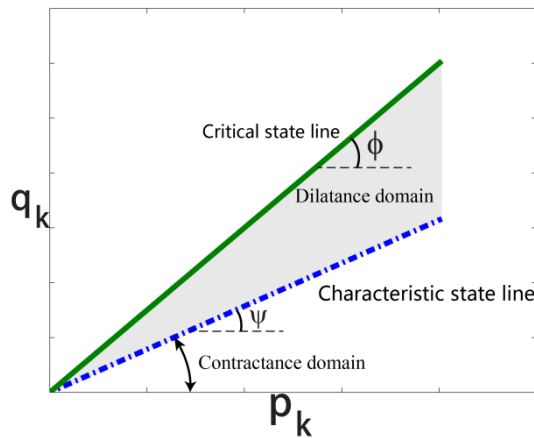


Figure 6: critical state line and characteristic state line.

The function $\zeta(r)$ allows to generate better the dilatancy law in order to define the limit of various behaviours of soil: zero for the very low strain ($\approx 10^{-5}$) until the low strain ($\approx 10^{-4}$). The plastic field is divided to three fields:

$$\zeta(r) = \begin{cases} 0 & \text{if } r \leq r_{hys} \text{ pseudo-elastic behavior} \\ \left(\frac{r - r_{hys}}{r_{mbl} - r_{hys}} \right)^m & \text{if } r_{mbl} \leq r \leq r_{hys} \text{ hysteretic behavior} \\ 1 & \text{if } r \geq r_{mbl} \text{ plastic mobilization} \end{cases} \quad [9]$$

2.2 Paraxial element

Simulating the seismic behaviour of a soil-column necessitates the use of a finite domain to represent the soil, and of either another domain or a boundary condition to represent the bedrock. The propagation of waves in any finite domain will create reflection waves that are undesired due to their absence in the reality of a semi-infinite domain. Numerical solutions need to be implemented in the simulation in order to mitigate or eliminate these fictive reflection waves. In earthquake engineering, the absorbent boundary is still a technical challenge due to its difficulty in the mathematical formulation to simulate the real local boundary in the soil.

Figure 7 is a schematic illustration of the problem. The seismic waves are generated by earthquake faults in an infinite elastic medium Ω_s , usually the semi-infinite bedrock. The modelled domain consists of an interior soil domain Ω_{in} , finite elastic domain Ω_s (a thin layer of bedrock below the soil) and the interface Σ along the outside of Ω_s . Ω_s can be simulated as a radiation condition at the base of the domain of interest (at the interface Σ) by absorbent elements which are called paraxial elements. These elements are implemented into *CyberQuake*.

Paraxial element allows any incident wave reaching the boundary (reflected or diffracted) to be evacuated from the study domain and therefore allows avoiding any artificial reflection on the interface Σ . To obtain the local impedance of soil, the development is performed on the elastodynamic equations in Fourier domain. The detailed mathematical formulation can be found in Benzenati and Modaressi (1994) and Modaressi (2003). In this section, the variational formulation will be described in one dimension in order to understand how paraxial element plays a role in the finite element method.

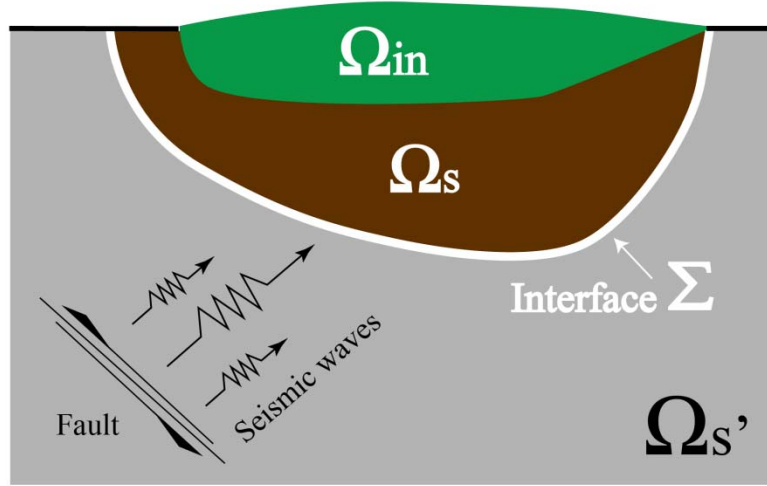


Figure 7: Schematic illustration of soil medium.

At the interface Σ between the two mediums Ω_s and $\Omega_{s'}$, the displacement and the stress vector should be continued:

$$\begin{cases} \underline{u}_s = \underline{u}_{s'} \\ \underline{\tau}_s + \underline{\tau}_{s'}(\underline{u}_{s'}) = 0 \end{cases} \quad [10]$$

$\underline{u}_{s'}$ is decomposed into two components, an incident wave field \underline{u}_i and a diffraction field \underline{u}_d :

$$\underline{u}_{s'} = \underline{u}_i + \underline{u}_d \quad [11]$$

In the medium $\Omega_{s'}$, the stress due to the diffraction is approached by the zero-order paraxial element for the stress vector at the interface Σ is :

$$\underline{\tau}_{s'}(\partial_t \underline{u}_{s'}) = \mathbf{A}_0(\partial_t \underline{u}_{s'}) = \rho \mathbf{C} \partial_t \underline{u}_{s'} \quad [12]$$

Where \mathbf{A}_0 is the paraxial operator that models approximately the stress vector in the elastic medium where the wave propagates in one direction. \mathbf{C} is the wave velocity tensor which is defined as

$$\mathbf{C} = \begin{bmatrix} c_s & 0 & 0 \\ 0 & c_s & 0 \\ 0 & 0 & c_p \end{bmatrix} \quad \text{where } c_s \text{ and } c_p \text{ are the shear wave velocity and pressure wave velocity,}$$

respectively.

It is assumed that the neighbourhood of interface Σ is linear elastic. After the zero-order approximation with Eq. [10] and Eq.[11], we can derive that:

$$\begin{aligned} \underline{\tau}_s &= -\underline{\tau}_{s'}(\underline{u}_{s'}) = -\underline{\tau}_{s'}(\underline{u}_i) - \underline{\tau}_{s'}(\underline{u}_d) \\ &\square -\underline{\tau}_{s'}(\underline{u}_i) - \mathbf{A}_0(\partial_t \underline{u}_d) \\ &\square -\underline{\tau}_{s'}(\underline{u}_i) - \mathbf{A}_0(\partial_t \underline{u}_{s'}) + \mathbf{A}_0(\partial_t \underline{u}_i) \end{aligned} \quad [13]$$

This equation represents the evolution of stress at the interface Σ . Both the stress field expressed as $\underline{\tau}_{s'}(\underline{u}_i)$ and the incoming wave velocity field $\mathbf{A}_0(\partial_t \underline{u}_i)$ are required. The variational formulation in

the virtual work principles with an admissible virtual work w is then written as follows and can be implemented in 1D FEM :

$$\int_{\Omega_s} \rho \partial_{tt} \underline{u}_s \cdot \underline{w} d\Omega + \int_{\Omega_s} \underline{\sigma}_s : \underline{\varepsilon}(\underline{w}) d\Omega + \int_{\Sigma} \mathbf{A}_0(\partial_t \underline{u}_s) \cdot \underline{w} d\Sigma =$$

$$\int_{\Omega_s} \rho \underline{g} \cdot \underline{w} d\Omega + \int_{\Sigma} (-\tau_{s'}(\underline{u}_t) + \mathbf{A}_0(\partial_t \underline{u}_t)) \cdot \underline{w} d\Sigma \quad [14]$$

3 One dimensional simulation for Grächen

As explained in the introduction, the aim of this report is to analyse the influence of soil mechanical characteristics on the response of a given site. Additionally, the influence of layers thickness (local variations) will be evaluated, indicating the sensibility of such methods to the number of available profiles. From borehole information of soil composition, an analysis was performed concerning the influence of various soil compositions, with emphasis on the layer of fine-grained lacustrine deposits. The influence of the mechanical characteristics of this layer on the response of the column is investigated by modifying these.

3.1 Input seisms characterisation

One dimensional analysis using *CyberQuake* was conducted to evaluate the influence of soil mechanical behaviour on site response. The accelerograms used in the simulation and their Fourier spectra are shown in Figure 8 and Figure 9, respectively.

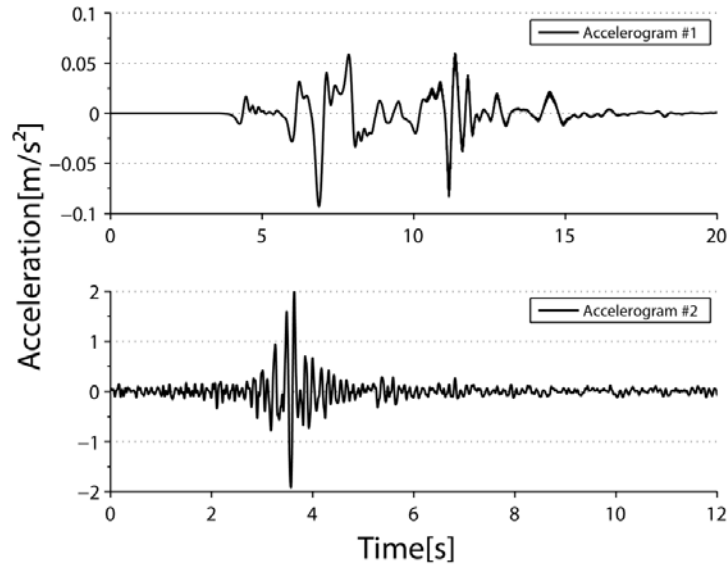


Figure 8: Input accelerations applied at outcropping bedrock.

The acceleration history #1 is provided by Swiss Seismological Service Institute of Geophysics (ETH Zurich). This is not a recorded ground motion but a synthetic seismogram obtained by applying the theory of fracture mechanics (Ely *et al.* 2009). The activated joint fault is supposed to create a magnitude 6 earthquake. The peak value of acceleration is 0.9 m/s^2 and frequency content is limited to frequencies lower than 3 Hz, which is an important limitation when compared to a real seism with broadband frequency content. Peak acceleration for an earthquake with a moment magnitude of 6 is

very low. This is due to the limitation of the model that generated this seismogram at the time these simulations were performed (see Task 2a.3).

The acceleration history #2 is taken from the library of *CyberQuake*. It is a real record of ground motion taken from the earthquake in Costa Rica on 07.08.1993. It has a peak value of acceleration equal to 2.02m/s^2 and its main frequency spectrum spreads from 0Hz to 20Hz, with main peaks at 5 and 8 Hz. Due to the limitations in #1, seism #2 is chosen as the reference input motion for the tests of soil columns performed in this study.

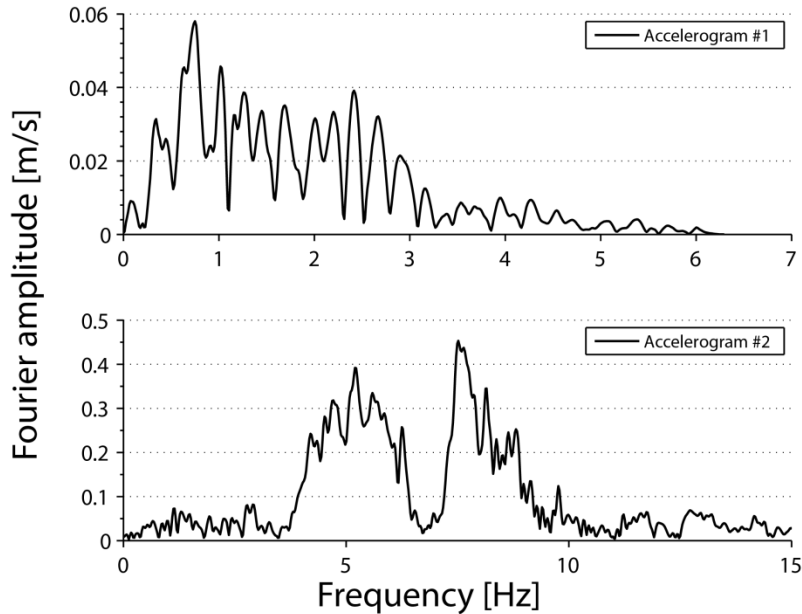


Figure 9: Fast Fourier spectrum of input accelerograms

3.2 Soil mechanical properties

Mechanical properties need to be estimated from two main sources, in the absence of sample testing. The characterization that is presented in Table 2 is based on the borehole geophysical information, enhanced by ambient noise measurements from Burjáněk (2010). These measurements lead to the determination of P-wave and S-wave velocities with depth at a location close to the boreholes, and therefore to an approximation of elastic properties. Two comparisons were performed: one on different materials and one on different profiles. The first test was conducted between the material No.1 and No.2 of Profile A. And the second test was conducted between the Profile B and Profile A with material No.1. Materials No.1 and No.2 differ by their elastic properties with a ratio of 2. Material No.1 is the case of a weak layer while material No.2 corresponds to a dense soil. This corresponds to the variability observed in the measurements that serve as a basis for this work, as seen in Figure 10.

In absence of laboratory tests, the non-linear behaviour parameters were set at usual values, with ϕ and ψ set at 30° . The other plastic and cyclic parameters were also set at usual values for silty sands: $r_{ela}=10^{-7}$, $r_{hys}=10^{-4}$, $r_{mbi}=10^{-3}$, $b=1$ and $\beta=10$ (Mellal 1997).

In addition to those variations in soil layers, several tests were conducted with various situations, as a rigid or deformable base and also with and without inclination of the soil column.

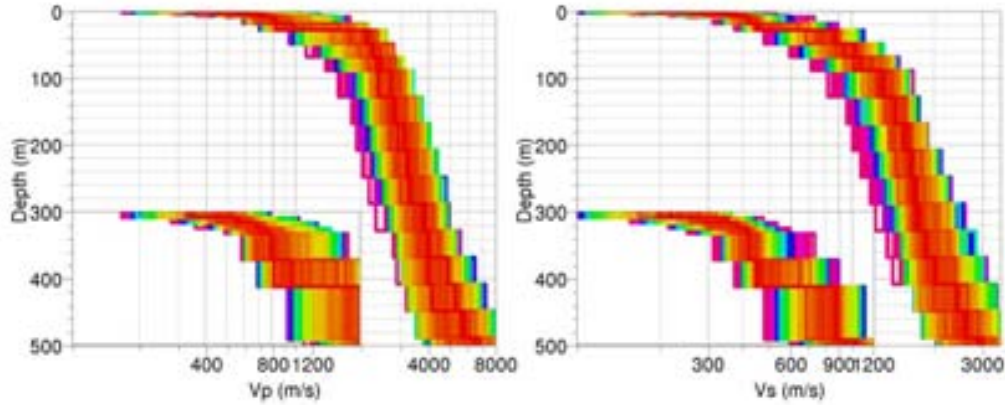


Figure 10: A set of inverted velocity profiles. First 50m are enlarged in the inset. Colours distinguish misfits' values.

Profiles A		Thickness[m]	Vs[m/s]	Vp[m/s]	ρ [kg/m ³]
Layer 1	Silty sand	7	180	340	1800
Layer 2	Sandy gravel	10	190	355	1800
Layer 3	Silty sand	5	190	360	1800
Layer 4	Silty sand (No.1/No.2)	28	145/290	280/560	1900
Bedrock	Bedrock	Infinite	800	1500	2100
Profiles B		Thickness[m]	Vs[m/s]	Vp[m/s]	ρ [kg/m ³]
Layer 1	Silty sand	7	180	340	1800
Layer 2	Silty sand	35	180	340	1800
Layer 3	Sandy gravel	15	190	355	1800
Layer 4	Silty sand	5	145	360	1800
Layer 5	Silty sand	14	145	560	1900
Bedrock	Bedrock	Infinite	800	1500	2100

Table 2: Material information of tests

3.3 Tests on constitutive models

A comparison between Hujoux model and elastic model was conducted to check the differences in the behaviour of soil materials as shown in Figure 11, showing Fourier transform of the surface accelerations. The accelerograms #1 was used for its reduced frequency content which allows to clearly identify the effect of a change in the constitutive model. The differences are enough to justify that the amplitude of the ground motion activates the non-linear behaviour of the soil, which is especially visible in the damping of high-frequency content (higher than 2 Hz). When soil behaves non-linearly (appearance of irreversible deformation), the shear rigidity will decrease, resulting in a decrease of shear wave velocity. The frequency of soil response is directly related to wave propagation. Therefore, the frequency of response will decrease and the frequency of a peak in Fourier

domain will decrease. This is observed in the second (~2.3 Hz) and third peak (~4 Hz) which are shifted towards lower frequency.

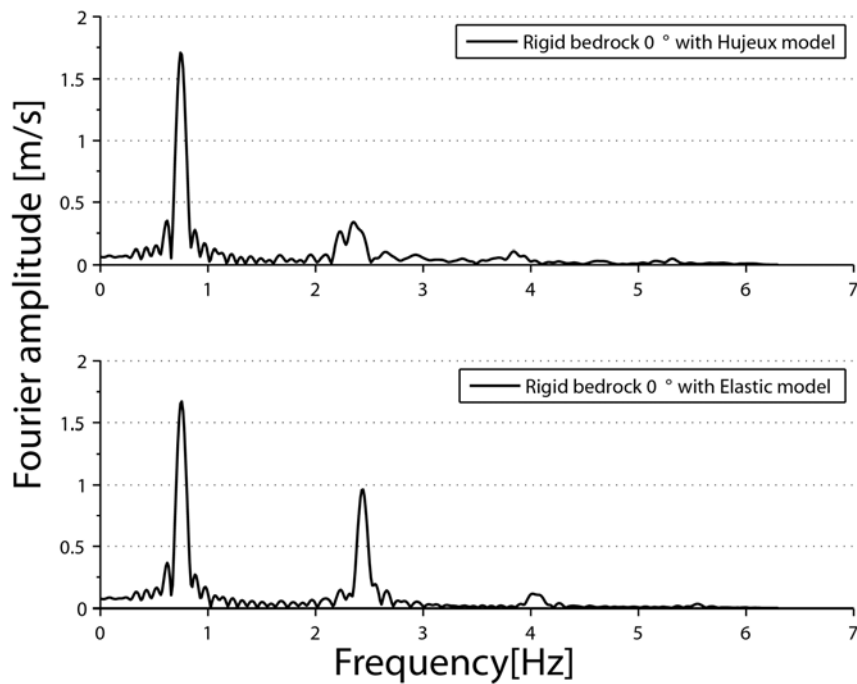


Figure 11 Fast Fourier transform of horizontal acceleration at surface to the accelerogram #1 with material No.1 in Profile A (from up to down: from up to down: soil column of Hujoux model; soil column of Elastic model)

3.4 Tests on soil materials

Figure 12 shows the Fourier transform spectrum of horizontal acceleration for two different cases on profile A, first with a layer made of material No.1 (so-called weak material) and the second with the same layer made of material No.2 (dense material). The difference is visible in both spectral content and peak Fourier amplitude. In the low frequencies, the soil with dense layer shows a peak value at about 1.5Hz and the one with lower modulus layer shows two smaller peak values at about 1Hz and 2.5Hz. A high energy at low frequencies could cause resonance effects to structures at the location, as the natural frequency of buildings often lies in that range. The lower modulus of material No.1 leads to potentially greater displacements (in the layer) but this contributes to a much larger energy dissipation through non-linear phenomena.

In terms of the coefficient of amplification (the ratio between peak value of ground acceleration at soil surface and peak acceleration of input motion), as shown in Figure 13, an attenuation (0.91) occurred in the test No.1 and an amplification (1.18) occurred in the test No.2. The explanation to this phenomenon is that the low modulus of very silty sands and silt materials making up this layer increased the energy damping in this layer, and globally attenuated the site response. Detailed analysis of Figure 12 shows that low and high frequencies are particularly damped, which is in line with the results of Bour *et al.* (2000).

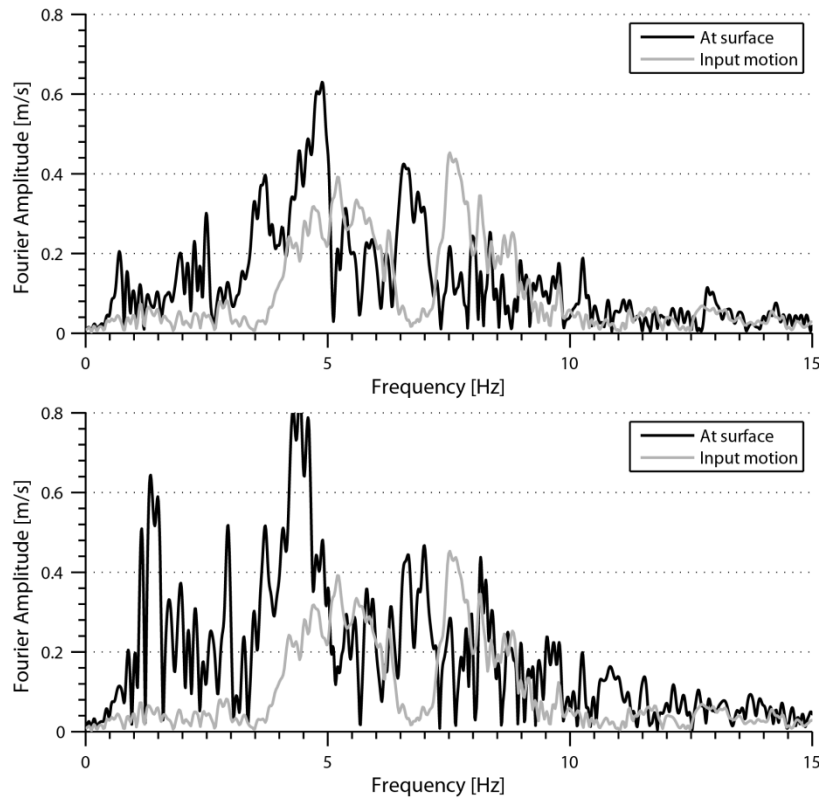


Figure 12: Fast Fourier spectrum of acceleration on Profile A. (above: test with material No.1 ; below: test with material No.2)

Another comparison, this time between two profiles is conducted. Figure 14 shows the Fourier spectrum of two profiles responses. Peak frequencies of both responses are different to that of input motion, which shows that a wide-spectra strong motion is a correct input to characterise the response of the soil column. The total depth of the soil layers is found to have less influence on site response than variations in soil characteristics. Profile B shows amplification in high frequencies, while these frequencies are more damped in both other cases. The response of profile 1 is more or less filtered out at high frequency due to its higher damping ratio on a thicker layer of soil.

It should be noticed that the hydrology conditions and the effect of liquefaction have not been taken into account in the present simulations. Loose silty sands in general are prone to liquefaction, in which case their behavior changes, what is not taken into account here. Soil profiles and wave-speed analysis tend to indicate medium-density materials with blocks, without impervious caps. These factors mitigate the risk of soil liquefaction.

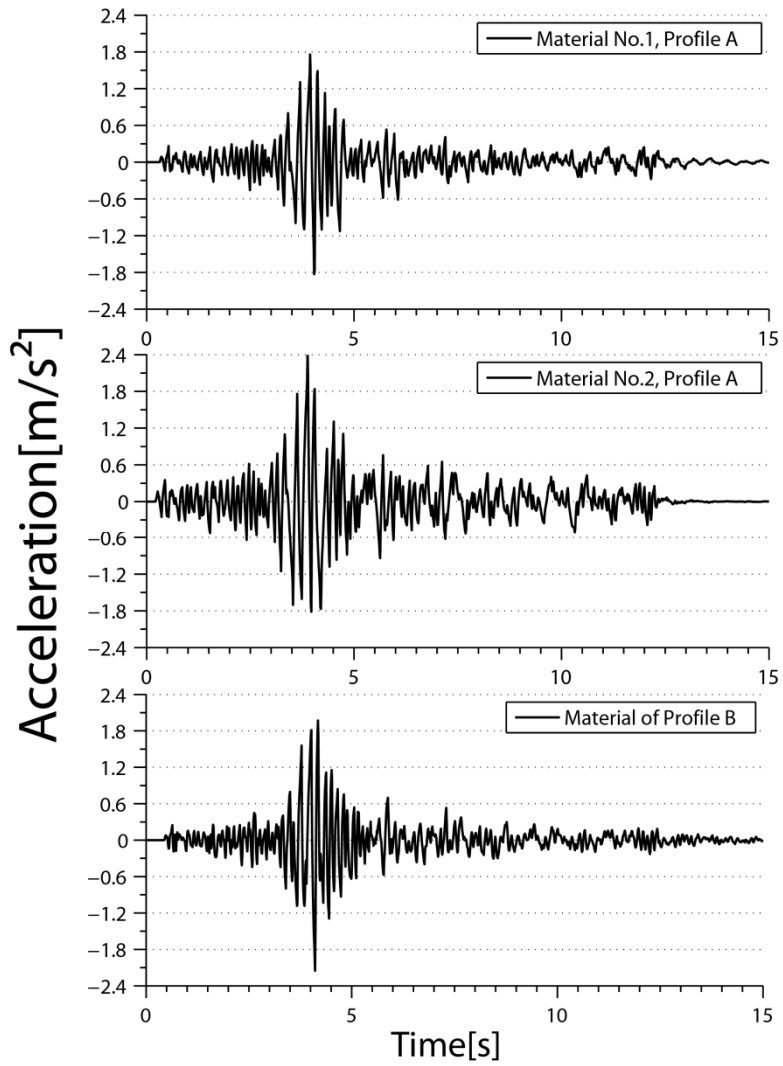


Figure 13: Acceleration at surface (above: material No.1, PGA=1.8m/s² , Amplification=0.91 ; middle: material No.2, PGA=2.4m/s², Amplification=1.18; below: Profile B, PGA=2.14m/s² , Amplification=1.06)

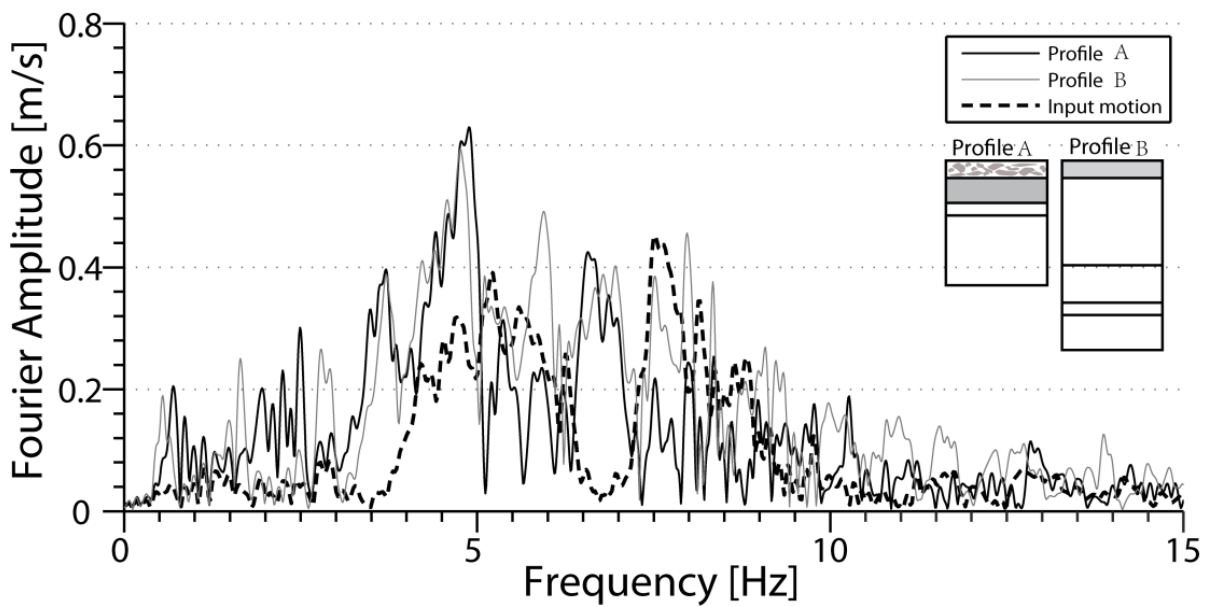


Figure 14: Fast Fourier responses of the accelerations for profile A and Profile B

In terms of acceleration, the profile A shows an amplification coefficient of 0.91 as mentioned before. And the profile B has an amplification coefficient of 1.06. There is almost no amplification effect to these two profiles in terms of peak acceleration value, but the difference between the two profiles nevertheless is significant, as well as the fact that one reduces the impact of the seism while the other slightly amplifies it.

3.5 Tests on inclinations and bedrocks

CyberQuake provides the possibility to analyse a soil column with an inclination, which can evaluate more realistic responses when soil column locates in the case of a slope, as found in the village of Grächen (illustrated in Figure 15). However, this function can be activated only with a rigid bedrock assumption. Main consequence is that in such case, reflected waves cannot be absorbed by paraxial elements. The inclination is defined as 10 degrees which is the slope angle of the village of Grächen. In such a case, the inclination is taken into account by separating the vertical and horizontal components of volume forces, the latter creating an initial shear stress $\tau_{yz,0}(z) = \rho g \sin(\alpha)z$, where α is the slope angle and z the depth. These elements are then used directly in the 1D vertical soil column model, with a reduced gravity $g_z = -g \cos(\alpha)$. However, the same simplification cannot be used for the paraxial formulation and this formulation cannot be used in 1D with an inclined bedrock.

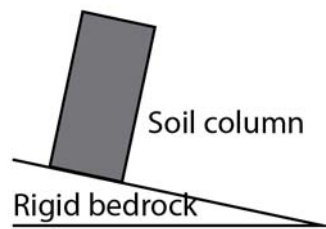


Figure 15 Illustration of soil column with an inclination

Figure 16 shows simulated responses of soil in terms of acceleration subjected to acceleration #1. An oscillation is observed with the rigid bedrock, which is dampened in the case of paraxial elements. This is because the rigid base assumption cannot eliminate reflecting waves in soil body. Consequently, the low-frequency oscillation observed after 8 seconds that can be observed in both two responses of rigid bedrock is not representative. The responses of the soil column with a rigid bedrock and a deformable bedrock before 8 seconds are very similar, as they are not affected by a reflected wave. The analysis will focus on these first 8 seconds.

There is no significant difference between the response without inclination and that with 10° inclination. This is mainly because of the small value of inclination angle, leading to $\cos(\alpha)$ being close to 1 and $\sin(\alpha)$ close to 0. This does not create significant initial shear stresses that could visibly influence the site response.

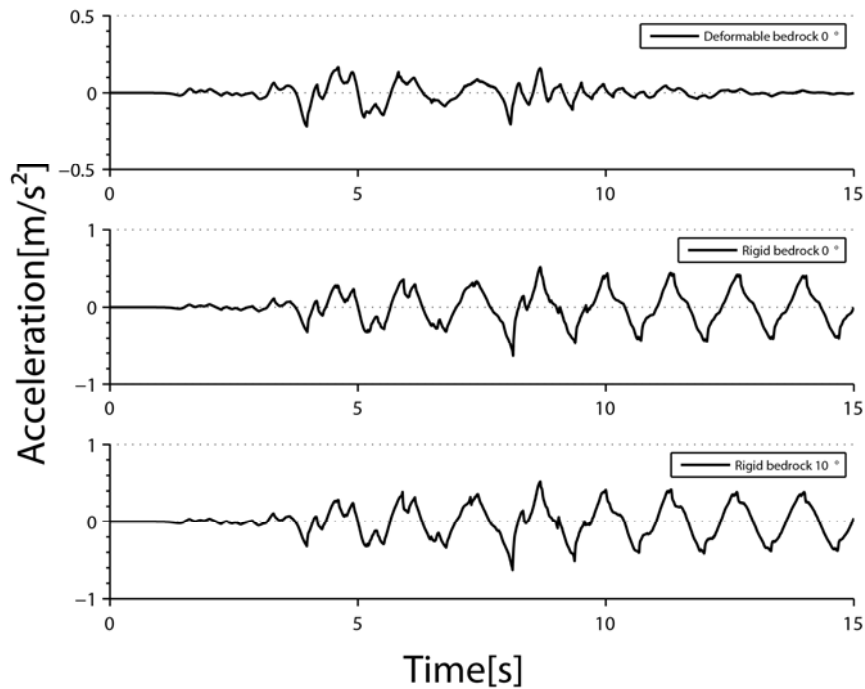


Figure 16: Response of horizontal acceleration at surface to the accelerogram #1 with material No.1 in Profile A (from up to down: soil column of deformable bedrock; rigid bedrock without inclination; rigid bedrock with 10° inclination)

Conclusion

In this study, a one-dimensional dynamic analysis using *CyberQuake* and a broadband input motion was performed between different materials and different profiles. The conditions for the validity of such a study were first investigated, highlighting the importance of boundary conditions. The effect of soil inclination was tested and found as minimal in the considered case. The results of this 1D dimensional study showed that a change in material characteristics in the less well-characterized deeper layers could significantly contribute to the global response of the soil column. A looser soil with lower rigidity induces a relatively high damping ratio, which results in dissipating more energy therefore attenuating soil response when wave propagates to the surface through soil layers. A correct prediction of the local behaviour of the site is therefore quite depending on the correct description of the materials, based on laboratory testing of undisturbed samples, which were not available for this study.

This effect was found to be more significant than the exact depth of the considered column and than material changes in uppermost layers. This was investigated by comparing results obtained on two different profiles that were based on actual boreholes. Though the resonance frequencies were found to be different, the overall magnitude and characteristics of surface ground motion were comparable between the cases profile A, material 1 and profile B.

The one-dimensional analysis provides a quantitative tool for estimating site effects and material properties under an earthquake scenario. However a one dimensional analysis cannot provide a clear view of site response to seismicity due to the presence of 3D effects such as surface and underground topography. A two dimensional analysis is considered as the second step of analysis. A more precise calibration of numerical parameters from laboratory investigation of undisturbed soil samples would

be necessary to validate the quantitative results of this study. The interdisciplinary nature of the project nevertheless made available measurements of wave-speeds in the considered site that were necessary to run this part of the project and to strongly restrict the range of values used in the study, rendering its results site-specific.

References

- Aubry, D., Hujeux, J.-C., Lassoudière, F. and Meimon, Y. (1982). *A double memory model with multiple mechanisms for cyclic soil behaviour*. Proceedings International Symposium on Numerical Models in Geomechanics, Zürich, A. A. Balkema.
- Benzenati, I. and Modaressi, H. (1994). Paraxial approximation for poroelastic media. *Soil Dynamics and Earthquake Engineering* **13**(2): 117-129.
- Bour, M., Chassagneux, D. and Mouroux, P. (2000). *Influence of a low resistance layer on seismic soil response using CyberQuake*. 12th World Conference on Earthquake Engineering, Auckland, NZ.
- Burjánek, J., Gassner-Stamm, G. and Fäh, D. (2010). *Array-measurements in the area of Visp and St. Niklaus*. COGEAR, Del. 3.1.2.
- Eichenberger, J., Ferrari, A., Schurmann, C. and Laloui, L. (2010). *Overview of existing data in the Matter valley (soil slopes)*. COGEAR, Del. 3b.3.1.
- Ely, G. P., Day, S. M. and Minster, J.-B. (2009). A support-operator method for 3-D rupture dynamics. *Geophysical Journal International* **177**(3): 1140-1150.
- Fäh, D. and COGEAR Working Group (2010). *Coupled Seismogenic Geohazards in Alpine Region*.
- Fritsche, S., Gisler, M., Schwarz, G., Fäh, D. and Kästli, P. (2010). *Historical earthquakes in the Valais*.
- Giardini, D., Wiemer, S., Fäh, D. and Deichmann, N. (2004). *Seismic hazard assessment of Switzerland*, Swiss Seismological Service.
- Hujeux, J. C. (1985). Une loi de comportement pour le chargement cyclique des sols. *Génie Parasismique*, V. Davidivici (Ed.). Paris, Presses ENPC, 287-302.
- Jaboyedoff, M., Baillifard, F. and Derron, M.-H. (2003). Preliminary note on uplift rates gradient, seismic activity and possible implications for brittle tectonics and rockslide prone areas: The example of western Switzerland. *Bulletin de la Société Vaudoise des Sciences Naturelles* **88**(3): 393-412.
- López-Caballero, F. (2003). *Influence du comportement non linéaire du sol sur les mouvements sismiques induits dans des géo-structures*. PhD thesis at Laboratoire des Mécanique des sols, Structures et Matériaux, Ecole central de Paris, France.
- Mellal, A. (1997). *Analyse des effets du comportement non linéaire des sols sur le mouvement sismique*. PhD thesis at Laboratoire des Mécanique des Sols, Structures et Matériaux, Ecole Centrale de Paris, France.
- Modaressi, A. (2003). *Modélisation des milieux poreux sous chargements complexes*. PhD thesis at LMSSMat, Ecole centrale de Paris.
- Modaressi, H. and Foerster, E. (2000). *CyberQuake: User's manual*, BRGM, France.
- Noverraz, F., Bonnard, C., Dupraz, H. and Huguenin, L. (1998). *Grands glissements de versants et climat — VERSINCLIM — Comportement passé, présent et futur des grands versants instables subactifs en fonction de l'évolution climatique, et évolution en continu des mouvements en profondeur*, Rapport final PNR 31. Zürich, VDF Hochschulverlag.

Deliverable 3b.3.6

- Roullé, A. and Bernardie, S. (2010). Comparison of 1D non-linear simulations to strong-motion observations: A case study in a swampy site of French Antilles (Pointe-à-Pitre, Guadeloupe). *Soil Dynamics and Earthquake Engineering* **30**(5): 286-298.
- Rovina, H. and Zuber, F. (1997). *Wasserbeschaffung für die Gemeinde Grächen Trinkwasserbohrungen in den Regionen „Meisen“ und „Taa“: Hydrogeologischer Bericht.*